SCNN: An Accelerator for Compressed-sparse Convolutional Neural Networks

Angshuman Parashar[†] Minsoo Rhu[†]
Anurag Mukkara[‡] Antonio Puglielli[*] Rangharajan Venkatesan[†] Brucek Khailany[†]
Joel Emer[†‡] Stephen W. Keckler[†] William J. Dally[†◇]

NVIDIA[†] Massachusetts Institute of Technology[‡] UC-Berkeley[*] Stanford University[◇]

arXiv:1708.04485v1 [cs.NE] 23 May 2017

***Abstract*—Convolutional Neural Networks (CNNs) have emerged as a fundamental technology for machine learning. High performance and extreme energy efficiency are critical for deployments of CNNs in a wide range of situations, especially mobile platforms such as autonomous vehicles, cameras, and electronic personal assistants. This paper introduces the Sparse CNN (SCNN) accelerator architecture, which improves performance and energy efficiency by exploiting the zero-valued weights that stem from network pruning during training and zero-valued activations that arise from the common ReLU operator applied during inference. Specifically, SCNN employs a novel dataflow that enables maintaining the sparse weights and activations in a compressed encoding, which eliminates unnecessary data transfers and reduces storage requirements. Furthermore, the SCNN dataflow facilitates efficient delivery of those weights and activations to the multiplier array, where they are extensively reused. In addition, the accumulation of multiplication products are performed in a novel accumulator array. Our results show that on contemporary neural networks, SCNN can improve both performance and energy by a factor of 2.7× and 2.3×, respectively, over a comparably provisioned dense CNN accelerator.**

I. Introduction

Driven by the availability of massive data and the computational capability to process it, deep learning has recently emerged as a critical tool for solving complex problems across a wide range of domains, including image recognition [20], speech processing [12], [16], [2], natural language processing [8], language translation [10], and autonomous vehicles [21]. Convolutional neural networks (CNNs) have become the most popular algorithmic approach for deep learning for many of these domains. Employing CNNs can be decomposed into two tasks: (1) training — in which the parameters of a neural network are learned by observing massive numbers of training examples, and (2) inference — in which a trained neural network is deployed in the field and classifies the observed data. Today, training is often done on GPUs [24] or farms of GPUs, while inference depends on the application and can employ CPUs, GPUs, FPGA, or specially-built ASICs.

During the training process, a deep learning expert will typically architect the network, establishing the number of layers, the operation performed by each layer, and the connectivity between layers. Many layers have parameters, typically filter weights, which determine their exact computation. The objective of the training process is to learn these weights, usually via a stochastic gradient descent-based excursion through the space of weights. This process typically employs a forward-propagation calculation for each training example, a measurement of the error between the computed and desired output, and then back-propagation through the network to update the weights. Inference has similarities, but only includes the forward-propagation calculation. Nonetheless, the computation requirements for inference can be prohibitively large, particularly with the emergence of deeper networks (hundreds of layers [17], [18], [26], [29]) and larger inputs sets, such as high-definition video. Furthermore, the energy efficiency of this computation is important, especially for mobile platforms, such as autonomous vehicles, cameras, and electronic personal assistants.

Recent published works have shown that common networks have significant redundancy and can be pruned dramatically during training without substantively affecting accuracy [15]. Our experience shows that the number of weights that can be eliminated varies widely across the layers but typically ranges from 20% to 80% [15], [14]. Eliminating weights results in a network with a substantial number of zero values, which can potentially reduce the computational requirements of inference.

The inference computation also offers a further optimization opportunity. In specific, many networks employ as their non-linear operator the ReLU (rectified linear unit) function which clamps all negative activation values to zero. The activations are the output values of an individual layer that are passed as inputs to the next layer. Our experience shows that for typical data sets, 50–70% of the activations are clamped to zero. Since the multiplication of weights and activations is the key computation for inference, the combination of these two

A version appears in the 44th IEEE/ACM International Symposium on Computer Architecture (ISCA-44), 2017.

This research was, in part, funded by the U.S. Government, under the DARPA CRAFT program. The views and conclusions contained in this document are those of the authors and should not be interpreted as representing the official policies, either expressed or implied, of the U.S. Government.

factors can reduce the amount of computation required by over an order of magnitude. Additional benefits can be achieved by a compressed encoding for zero weights and activations, thus allowing more to fit in on-chip RAM and eliminating energy-costly DRAM accesses.

In this paper, we introduce the Sparse CNN (SCNN) accelerator architecture, a new CNN inference architecture that exploits both weight and activation sparsity to improve both performance and power. Previous works have employed techniques for exploiting sparsity, including saving computation energy for zero-valued activations and compressing weights and activations stored in DRAM [7], [6]. Other works have used a compressed encoding of activations [1] or weights [30] in parts of their dataflow to reduce data transfer bandwidth and save time for computations of some multiplications with a zero operand. While these prior architectures have largely focused on eliminating computations and exploiting some data compression, SCNN couples an algorithmic dataflow that eliminates all multiplications with a zero operand while employing a compressed representation of both weights and activations through almost the entire computation.

At the heart of the SCNN design is a processing element (PE) with a multiplier array that accepts a vector of weights and a vector of activations. Unlike previous convolutional dataflows [5], [11], [7], [25], the SCNN dataflow only delivers weights and activations to the multiplier array that can all be multiplied by one another in the manner of a *Cartesian product*. Furthermore, the activation vectors are reused in an *input stationary* [6] fashion against a number of weight vectors to reduce data accesses. Finally, only non-zero weights and activations are fetched from the input storage arrays and delivered to the multiplier array. As with any CNN accelerator, SCNN must accumulate the partial products generated by the multipliers. However, since the products generated by the multiplier array cannot be directly summed together, SCNN tracks the output coordinates associated with each multiplication and sends the coordinate and product to a scatter accumulator array for summing.

To increase parallelism beyond a single PE, multiple PEs can be run in parallel with each working on a disjoint 3D *tile* of input activations. Because of the end-to-end compression of activations, SCNN can keep the both the input and output activations of each tile local to its PE, further reducing energy-hungry data transmission. Overall, this results in a design with efficient compressed storage and delivery of input operands, high reuse of the input operands in the multiplier array, and that spends no time on multiplications with zero operands.

To evaluate SCNN, we developed a cycle-level performance model and a validated analytical model that allows us to quickly explore the design space of different types of accelerators. We also implemented an SCNN PE in synthesizable System C and compiled the design into gates using a combination of commercial high-level synthesis (HLS) tools and a traditional verilog compiler. Our results show that 64 PE SCNN implementation with 16 multipliers per PE (1024 multipliers in total) can be implemented in approximately $7.9mm^2$, which is somewhat larger than an equivalently provisioned dense accelerator architecture due to the overheads of managing the sparse dataflow. On a range of networks, SCNN provides a factor of 2.7× speedup and a 2.3× energy reduction relative to the dense architecture.

TABLE I
NETWORK CHARACTERISTICS. WEIGHTS AND ACTIVATIONS ASSUME A DATA-TYPE SIZE OF TWO BYTES.

Network	# Conv. Layers	Max. Layer Weights	Max. Layer Activations	Total # Multiplies
AlexNet [20]	5	1.73 MB	0.31 MB	0.69 B
GoogLeNet [28]	54	1.32 MB	1.52 MB	1.1 B
VGGNet [27]	13	4.49 MB	6.12 MB	15.3 B

II. MOTIVATION

Convolutional Neural Network algorithms (CNNs) are essentially a cascaded set of pattern recognition filters trained with supervision [21]. A CNN consists of a series of layers, which include convolutional layers, non-linear scalar operator layers, and layers that downsample the intermediate data, for example by pooling. The convolutional layers represent the core of the CNN computation and are characterized by a set of filters that are usually 1×1 or 3×3, and occasionally 5×5 or larger. The values of these filters are the *weights* that are trained using a training set for the network. Some deep neural networks (DNNs) also include fully-connected layers, typically toward the end of the DNN. During inference, a new image (in the case of image recognition) is presented to the network, which classifies into the training categories by computing in succession each of the layers in the network. The intermediate data between the layers are called *activations* and the output activation of one layer becomes the input activation of the next layer. In this paper, we focus on accelerating the convolutional layers as they constitute the majority of the computation [9].

Table II lists the attributes of three commonly used networks in image processing: AlexNet [20], GoogLeNet [28], and VGGNet [27], whose specifications come from the Caffe BVLC Model Zoo [4]. The increasing layer depth across the networks represents the successively more accurate networks in the ImageNet [19] competition. The Maximum Weights and Activations columns indicate the size of the largest weight and activation matrices across the layer of the network. The last column lists the total number of multiplies required to compute a single inference pass through all of the convolutional layers of the network. These data and computational requirements are derived from the standard ImageNet inputs images of 224×224 pixels. Processing larger, higher resolution images will result in greater computational and data requirements.

Sparsity in CNNs. Sparsity in a layer of a CNN is defined as the fraction of zeros in the layer's weight and input activation matrices. The primary technique for creating weight sparsity is to prune the network during training. Han, et al. developed a pruning algorithm that operates in two

phases [15]. First, any weight with an absolute value that is close to zero (e.g. below a defined threshold) is set to zero. This process has the effect of removing weights from the filters, and sometimes even forcing an output activation to always to be zero. Second, the remaining network is retrained, to regain the accuracy lost through naïve pruning. The result is a smaller network with accuracy extremely close to the original network. The process can be iteratively repeated to reduce network size while maintaining accuracy.

Activation sparsity occurs dynamically during inference and is highly dependent on the data being processed. Specifically, the rectified linear unit (ReLU) function that is commonly used as the non-linear operator in CNNs forces all negatively valued activations to be clamped to zero. After completing computation of a convolutional layer, a ReLU function is applied point-wise to each element in the output activation matrices before the data is passed to the next layer.

To measure the weight and activation sparsity, we used the Caffe framework [3] to prune and train the three networks listed in Table II, using the pruning algorithm of [15]. We then instrumented the Caffe framework to inspect the activations between the convolutional layers. Figure 1 shows the weight and activation density (fraction of non-zeros or complement of sparsity) of the layers of the networks, referenced to the left-hand y-axes. As GoogLeNet has 54 convolutional layers, we only show a subset of representative layers. The data shows that weight density varies across both layers and networks, reaching a minimum of 30% for some of the GoogLeNet layers. Activation density also varies, with density typically being higher in early layers. Activation density can be as low as 30% as well. The triangles shows the ideal amount of work (measured in multiplies of non-zero values) that could be achieved through maximum exploitation of sparsity by taking the product of the weight and activation densities on a per-layer basis. Typical layers can reduce work by a factor of 4, and can reach as high as a factor of ten.

Exploiting sparsity. Since multiplication by zero just results in a zero, it should require no work. In addition, that zero will contribute nothing to the partial sum it is part of, so the addition is unnecessary as well. Furthermore, data with many zeros can be represented in a compressed form. Together these characteristics provide a number of opportunities for optimization:

- **Compressing data:** Encoding the sparse weights and/or activations provides an architecture an opportunity to reduce the amount of data that must be moved throughout the memory hierarchy. It also reduces the data footprint, which allows larger matrices to be held a given size storage structure.
- **Eliminating computation:** For multiplications that have a zero weight and/or activation operand, the operation can be data gated or the operands might never be sent to the multiplier. This can save energy consumption or both time and energy consumption, respectively.

Our SCNN architecture exploits both these opportunities. First, it employs a dense encoding of sparse weights and activations. Second, it uses a novel dataflow that delivers only those densely encoded weights and activations to the multipliers.

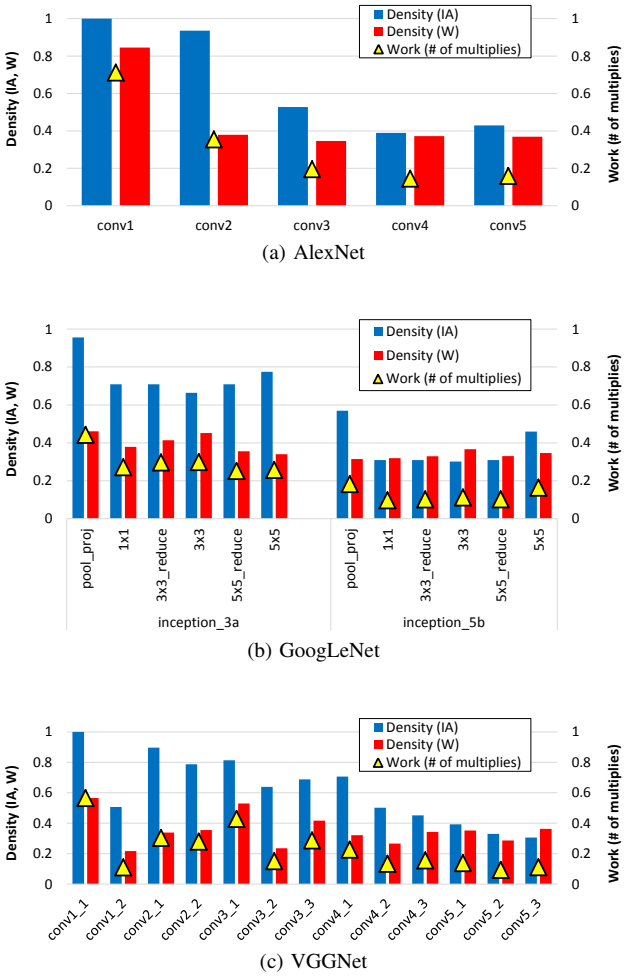

Fig. 1. Input activation and weight density and the reduction in the amount of work achievable by maximally exploiting sparsity.

III. SCNN Dataflow

The core operation in a CNN convolutional layer is a 2-dimensional sliding-window convolution of an $R \times S$ element *filter* over a $W \times H$ element *input activation* plane to produce a $W \times H$ element *output activation* plane. There can be multiple (C) input activation planes, which are referred to as *input channels*. A distinct filter is applied to each input activation channel, and the filter output for each of the C channels are accumulated together element-wise into a single output activation plane. Multiple filters (K) can be applied to the same body of input activations to produce K *output channels* of activations. Finally, a batch of length N of groups of C channels of input activation planes can be applied to the same volume of filter weights. Figure 2 shows these parameters applied to the computation of a single CNN layer.

The set of computations for the complete layer can be formulated as a loop nest over these 7 variables. Because

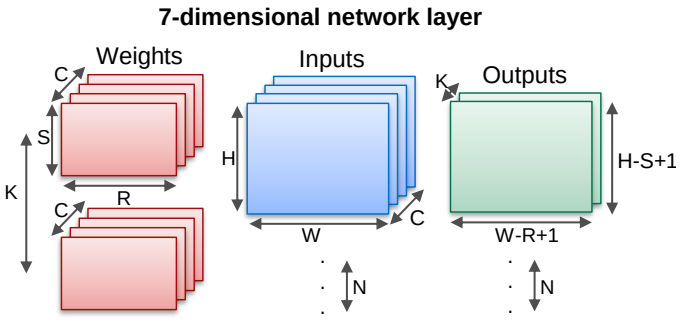

Fig. 2. CNN computations and parameters.

```
for n = 1 to N
  for k = 1 to K
    for c = 1 to C
      for w = 1 to W
        for h = 1 to H
          for r = 1 to R
            for s = 1 to S
              out[n][k][w][h] +=
                in[n][c][w+r-1][h+s-1] *
                filter[k][c][r][s];
```

Fig. 3. 7-dimensional CNN loop nest.

multiply-add operations are associative (modulo rounding errors, which we will ignore in this study), all permutations of these 7 loop variables are legal. Figure 3 shows an example loop nest based on one such permutation. We can concisely describe this nest as $N \rightarrow K \rightarrow C \rightarrow W \rightarrow H \rightarrow R \rightarrow S$. Each point in the 7-dimensional space formed from these variables represents a single multiply-accumulate operation. Note that for the remainder of this paper, we assume a batch size of 1, which is common for inferencing tasks.

This simple loop nest can be transformed in numerous ways to capture different reuse patterns of the activations and weights and to map the computation to a hardware accelerator implementation. A CNN's *dataflow* defines how the loops are ordered, partitioned, and parallelized [6]. Prior work[6] has shown that the choice of dataflow has a significant impact on the area and energy-efficiency of an architecture. In fact, the choice of dataflow is perhaps the single most significant differentiator between many prior works on CNN architectures.

While the concept of dataflow has been studied for dense architectures, sparse architectures can also employ various alternative dataflows, each with its own set of trade-offs. While an exhaustive enumeration of sparse dataflows is beyond the scope of this paper, we present a specific dataflow called *PlanarTiled-InputStationary-CartesianProduct-sparse* (or PT-IS-CP-sparse). After examining a range of different dataflows, we selected PT-IS-CP-sparse because it enables reuse patterns that exploit the characteristics of sparse weights and activations. This section first presents an equivalent dense dataflow (PT-IS-CP-dense) to explain the decomposition of the computations and then adds the specific features for PT-IS-CP-sparse .

A. The PT-IS-CP-dense Dataflow

Single-multiplier temporal dataflow. To understand the *temporal* component of the PT-IS-CP-dense dataflow, consider the operation of a *processing element* (or PE) with a single multiply-accumulate unit. The dataflow employs an *input-stationary* computation order in which an input activation is held stationary at the computation units as it is multiplied by all the filter weights needed to make all its contributions to each of the the K output channels (a $K \times R \times S$ subvolume). Thus each input activation will contribute to a volume of $K \times R \times S$ output activations. This order maximizes the reuse of the input activations, while paying a cost to stream the weights to the computation units. Accommodating multiple input channels (C) adds an additional outer loop and results in the loop nest $C \rightarrow W \rightarrow H \rightarrow K \rightarrow R \rightarrow S$.

The PT-IS-CP-dense dataflow requires input buffers for weights and input activations, and a accumulator buffer to store the *partial sums* of the output activations. The accumulator buffer must perform a read-add-write operation for every access to a previously-written index. We call this accumulator buffer along with the attached adder an *accumulation unit*.

Parameters of contemporary networks cause these buffers to be large and energy-expensive to access. The input-stationary temporal loop nest amortizes the energy cost of accessing the input buffer over multiple weight and accumulator buffer accesses. More precisely, the register in which the stationary input is held over $K \times R \times S$ iterations serves as an inner buffer filtering accesses to the larger input buffer.

Unfortunately, the stationarity of input activations comes at the cost of more streaming accesses to the weights and partial sums (in the accumulator buffer). Blocking the weights and partial sums in the output channel (K) dimension can increase reuse of these data structures and improve energy efficiency. We factor the output channel variable (K) into K_c (which we call a *output-channel group*) and K/K_c, and only store weights and outputs for a single output-channel group at a time inside the weight and accumulator buffers. Thus the subvolumes that are housed in buffers at the computation unit are:

- Weights: $C \times K_c \times R \times S$
- Inputs: $C \times W \times H$
- Partial Sums: $K_c \times W \times H$

An outer loop over all the K/K_c output-channel chunks results in the complete loop nest $K/K_c \rightarrow C \rightarrow W \rightarrow H \rightarrow K_c \rightarrow R \rightarrow S$. Note that each iteration of this outer loop will require the weight buffer to be refilled and the accumulator buffer must be drained and cleared, while the contents of the input buffer will be fully reused because the same input activations are used across all output channels.

Intra-PE parallelism. To exploit the parallelism of many multipliers within a PE, we fetch a vector of F filter-weights

from the weight buffer and a vector of I inputs from the input activation buffer. These values are delivered to an array of $F \times I$ multipliers to compute a full Cartesian product of output partial-sums. Each product yields a useful partial sum such that no extraneous fetches or computations are performed. PT-IS-CP-sparse will exploit this same property to make computation efficient on compressed-sparse weights and input activations.

The multiplier outputs are sent to the accumulation unit, which updates the partial sums of the output activation. Each multiplier output is accumulated with a partial sum at the matching output coordinates in the output activation space. These coordinates are computed in parallel with the multiplications. The accumulation unit must employ at least $F \times I$ adders to match the throughput of the multipliers. Figure 4 shows pseudo-code for the PT-IS-CP-dense dataflow, including blocking in the K dimension (A,C), fetching vectors of input activations and weights (B,D), and computing the Cartesian product in parallel (E,F). The $Kcoord()$, $Xcoord()$, and $Ycoord()$ functions compute the k, x, and y coordinates of the uncompressed output volume using a de-linearization of the temporal loop indices a and w, the spatial loop indices i and f, and the known filter width and height. Note that this dataflow is simply a reordered, partitioned and parallelized version of Figure 3.

Inter-PE parallelism. To scale beyond the practical limits of multiplier count and buffer sizes within a PE, we employ a tiling strategy to spread the work across an array of PEs so that each PE can operate independently. PT-IS-CP-dense partitions the $W \times H$ element activation plane into smaller $W_t \times H_t$ element *tiles* that are distributed across the PEs. Each tile extends fully into the input-channel dimension C, resulting in an input-activation volume of $C \times W_t \times H_t$ assigned to each PE. Weights are broadcast to the PEs and each PE operates on its own subset of the input and output activation space.

Unfortunately, strictly partitioning both input and output activations into $W_t \times H_t$ tiles does not work because the sliding-window nature of the convolution operation introduces cross-tile dependencies at tile edges. These dependencies are called *halos*. Halos can be resolved in two ways:

- **Input halos:** The input buffers at each PE are sized to be slightly larger than $C \times W_t \times H_t$ to accommodate the halos. These halo input values are replicated across adjacent PEs, but outputs are strictly private to each PE. Replicated input values can be multicast when they are being fetched into the buffers.
- **Output halos:** The output buffers at each PE are sized to be slightly larger than $K_c \times W_t \times H_t$ to accommodate the halos. The halos now contain incomplete partial sums that must be communicated to neighbor PEs for accumulation. This communication occurs at the end of computing each output-channel group.

Our PT-IS-CP-dense dataflow uses output halos, though the efficiency difference between the two approaches is minimal.

```
    BUFFER wt_buf[C][Kc*R*S/F][F];
    BUFFER in_buf[C][Wt*Ht/I][I];
    BUFFER acc_buf[Kc][Wt+R-1][Ht+S-1];
    BUFFER out_buf[K/Kc][Kc*Wt*Ht];
(A) for k' = 0 to K/Kc-1
    {
      for c = 0 to C-1
        for a = 0 to (Wt*Ht/I)-1
        {
(B)       in[0:I-1] = in_buf[c][a][0:I-1];
(C)       for w = 0 to (Kc*R*S/F)-1
          {
(D)        wt[0:F-1] = wt_buf[c][w][0:F-1];
(E)        parallel_for (i=0 to I-1) x (f=0 to F-1)
           {
             k = Kcoord(w,f);
             x = Xcoord(a,i,w,f);
             y = Ycoord(a,i,w,f);
(F)          acc_buf[k][x][y] += in[i]*wt[f];
           }
          }
        }
      out_buf[k'][0:Kc*Wt*Ht-1] =
        acc_buf[0:Kc-1][0:Wt-1][0:Ht-1];
    }
```

Fig. 4. PT-IS-CP-dense dataflow.

B. PT-IS-CP-sparse Dataflow

PT-IS-CP-sparse is a natural extension of PT-IS-CP-dense that exploits sparsity in the weights and input activations. The dataflow is specifically designed to operate on compressed-sparse encodings of the weights and input activations and to produce a compressed-sparse encoding of the output activations. At a CNN layer boundary, the output activations of the previous layer become the input activations of the next layer. While prior work has proposed a number of compressed-sparse representations [13], [1], [30], the specific format used is orthogonal to the sparse architecture itself. What is key is that decoding a sparse format ultimately yields a non-zero data value and an index indicating the coordinates of the value in the weight or input activation matrices.

To facilitate easier decoding of the compressed-sparse blocks, weights are grouped into compressed-sparse blocks at the granularity of an output-channel group, with of $K_c \times R \times S$ weights encoded into one compressed block. Likewise, input activations are encoded at the granularity of input channels, with a block of $W_t \times H_t$ encoded into one compressed block. At each access, the weight buffer delivers a vector of F **non-zero** filter weights along with each of their coordinates within the $K_c \times R \times S$ region. Similarly, the input buffer delivers a vector of F **non-zero** input activations along with each of their coordinates within the $W_t \times H_t$ region. Similar to the dense dataflow, the multiplier array computes the full cross-product of $F \times I$ partial sum outputs, with no extraneous computations. Unlike a dense architecture, output coordinates are not derived from loop indices in a state machine but from the coordinates of non-zero values embedded in the compressed format.

Even though calculating output coordinates is trivial, the multiplier outputs are not typically contiguous as they are in PT-IS-CP-dense. Thus the $F \times I$ multiplier outputs must be

scattered to discontiguous addresses within the $K_c \times W_t \times H_t$ output range. Because any value in the output range can be non-zero, the accumulation buffer must be kept in a dense format. In fact, output activations will probabilistically have high density even with a very low density of weights and input activations, until they pass through a ReLU operation.

To accommodate the needs of accumulation of sparse partial sums, we modify the monolithic $K_c \times W_t \times H_t$ accumulation buffer from the PT-IS-CP-dense dataflow into a distributed array of smaller accumulation buffers accessed via a scatter network which can be implemented as a crossbar switch. The scatter network routes an array of $F \times I$ partial sums to an array of A accumulator banks based on the output index associated with each partial sum. Taken together, the complete accumulator array still maps the same $K_c \times W_t \times H_t$ address range, though the address space is now split across a distributed set of banks. PT-IS-CP-sparse can be implemented via small adjustments of Figure 4. Instead of a dense vector fetches, (B) and (D) fetch the compressed sparse input activations and weights, respectively. In addition, the coordinates of the non-zero values in the compressed-sparse form of these data structures must be fetched from their respective buffers (not shown). After that the accumulator buffer (F) must be indexed with the computed output coordinates from the sparse weight and activations. Finally, when the computation for the output-channel group has been completed the accumulator buffer is drained and compressed into the next level of buffer.

IV. SCNN Architecture

A complete SCNN accelerator employing the PT-IS-CP-sparse dataflow of Section III consists of multiple SCNN processing elements (PEs) connected via simple interconnections. Figure 5 shows an array of PEs, with each PE including channels for receiving weights and input activations, and channels delivering output activations. The PEs are connected to their nearest neighbors to exchange halo values during the processing of each CNN layer. The PE array is driven by a layer sequencer to orchestrate the movement of weights and activations and is connected to a DRAM controller that can broadcast weights to the PEs and stream activations to/from the PEs.

Processing Element (PE) Architecture. Figure 6 shows the microarchitecture of an SCNN PE, including a weight buffer, input/output activation RAMs (IARAM and OARAM), a multiplier array, a scatter crossbar, a bank of accumulator buffers, and a post-processing unit (PPU). To process the first CNN layer, the layer sequencer streams a portion of the input image into the IARAM of each PE and broadcasts the compressed-sparse weights into the weight buffer of each PE. Upon completion of the layer, the sparse-compressed output activation is distributed across the OARAMs of the PEs. When possible, the activations are held in the IARAMs/OARAMs and are never swapped out to DRAM. If the output activation volume of a layer can serve as the input activation volume for the next layer, the IARAMs and OARAMs are logically swapped between the two layers' computation sequences.

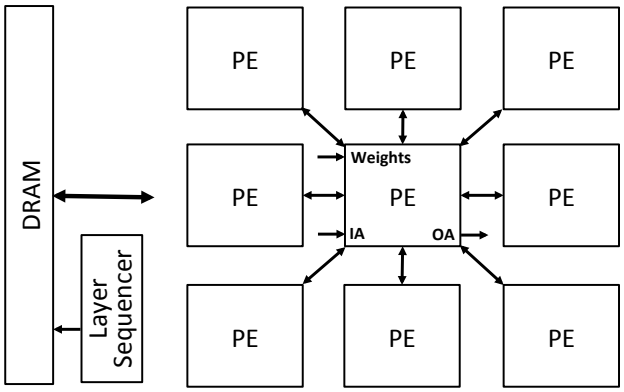

Fig. 5. Complete SCNN architecture.

Each PE's state machine operates on the weight and input activations in the order defined by the PT-IS-CP-sparse dataflow to produce an output-channel group of $K_c \times W_t \times H_t$ partial sums inside the accumulation buffers. First, a vector F of compressed weights and a vector I of compressed input activations are fetched from their respective buffers. These vectors are distributed into the $F \times I$ multiplier array which computes a form of the cartesian product of the vectors. At the same time, the indices from the sparse-compressed weights and activations are processed to compute the coordinates in dense output activation. The $F \times I$ products are delivered to an array of A accumulator banks, indexed by the output coordinates. To reduce contention among products that hash to the same accumulator bank, A is set to be larger than $F \times I$. Our results show that $A = 2 \times F \times I$ sufficiently reduces accumulator bank contention. Each accumulator bank includes adders and small set of entries for the output channels associated with the output-channel group being processed. The accumulation buffers are double-buffered so that one set of banks can be updated by incoming partial sums while the second set of banks are drained out by the PPU. When the output-channel group is complete, the PPU performs the following tasks: (1) exchange partial sums with neighbor PEs for the halo regions at the boundary of the PE's output activations, (2) apply the non-linear activation (e.g. ReLU), pooling, and dropout functions, and (3) compress the output activations into the compressed-sparse form and write them into the OARAM.

SCNN uses a simple compressed-sparse encoding approach based on run-length encoding scheme. The index vector encodes the number of zeros between each element in the compressed-sparse data vector. Determining the coordinates in the accumulator buffer for each multiplier output requires reading the index vectors for F and I and combining them with the coordinates of portion of the output activation space currently being processed. Four bits per index allows for up to 15 zeros to appear between any two non-zero elements. Non-zero elements that are further apart can have a zero-value placeholder without incurring any noticable degradation in compression efficiency.

While SCNN will operate most efficiently when the activa-

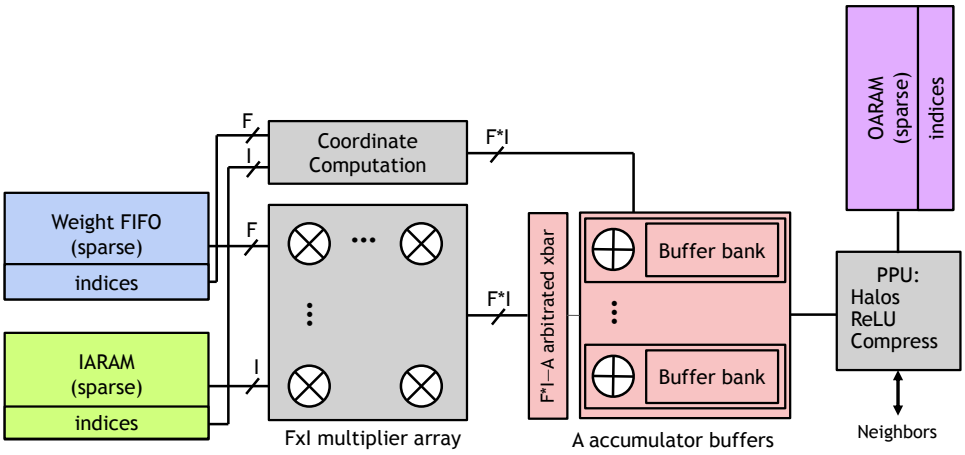

Fig. 6. SCNN PE employing the PT-IS-CP-sparse dataflow.

TABLE II
SCNN DESIGN PARAMETERS.

PE Parameter	Value
Multiplier width	16 bits
Accumulator width	24 bits
IARAM/OARAM (each)	10KB
Weight FIFO	50 entries (500 B)
Multiply array ($F \times I$)	4×4
Accumulator banks	32
Accumulator bank entries	32
SCNN Parameter	**Value**
# PEs	64
# Multipliers	1024
IARAM + OARAM data	1MB
IARAM + OARAM indices	0.2MB

TABLE III
SCNN PE AREA BREAKDOWN.

PE Component	Size	Area (mm^2)
IARAM + OARAM	20 KB	0.031
Weight FIFO	0.5 KB	0.004
Multiplier array	16 ALUs	0.008
Scatter network	16×32 crossbar	0.026
Accumulator buffers	6 KB	0.036
Other	—	0.019
Total	—	0.123
Accelerator total	64 PEs	7.9

tions fit in the on-chip activation RAMs, Large networks, such as VGGNet, require activations to be saved to and restored from DRAM. CNN accelerator architectures such as SCNN can employ a tiling approach that operates on a 2D subset of the activation space at a time. Our analysis shows that for both dense and sparse architectures, the DRAM accesses for one tile can be hidden by pipelining them in tandem with the computation of another tile. While we do not present the details of the tiled approach here, we do account for the DRAM access energy overhead for tiling in Section VI.

SCNN Architecture Configuration. While the SCNN architecture can be scaled across a number of dimensions, Table II lists the key parameters of the SCNN design we explore in this paper. The design employs an 8×8 array of PEs, each with a 4×4 multiplier array, and an accumulator buffer with 32 banks. We chose a design point of 1,024 multipliers to match the expected computation throughput required to process HD video in real-time at acceptable frame rates. The IARAM and OARAM are sized so that the sparse activations of AlexNet and GoogleNet can fit entirely within these RAMs so that activations need not spill to DRAM. The weight FIFO and the activation RAMs each carry a 10-bit overhead for each 16-bit value to encode the coordinates in the compressed-sparse format. In total, the SCNN design includes a total of 1,024 multipliers and 1MB of activation RAM. At the synthesized clock speed of the PE of slightly more than 1 GHz, this design achieves a peak throughput of 2 Tera-ops (16-bit multiplies plus 24-bit adds).

Area Analysis. To prototype the SCNN architecture, we designed an SCNN PE in synthesizable SystemC and then used the Catapult high-level synthesis (HLS) tool [23], [22] to generate Verilog RTL. During this step, we used HLS design constraints to optimize the design by mapping different memory structures to synchronous RAMs and latch arrays and pipelining the design to achieve full throughput. We then used Synopsys Design Compiler to perform placement-aware logic synthesis and obtain post-synthesis area estimates in a TSMC 16nm FinFET technology. Table III summarizes the area of the major structures of the SCNN PE. A significant fraction of the PE area is contributed by memories (IARAM, OARAM, accumulator buffers), which consume 57% of the PE area, while the multiplier array only consumes 6%. IARAM and OARAM are large in size and consume 25% of the PE area. Accumulator buffers, though smaller in size compared to IARAM/OARAM, are heavily banked (32 banks), contributing to their large area.

V. EXPERIMENTAL METHODOLOGY

CNN performance and power measurements. To model

the performance of the SCNN architecture, we rely primarily on a custom-built cycle-level simulator. This simulator is parameterizable across dimensions including number of processing element (PE) tiles, RAM capacity, multiplier array dimensions (F and I), and accumulator buffers (A). The SCNN simulator is driven by the pruned weights and sparse input activation maps extracted from the Caffe Python interface (pycaffe) [3] and executes each layers of the network one at a time. As a result, the simulator captures the effects of the sparsity of the data and its effect on load balancing within the SCNN architecture.

We also developed TimeLoop, a detailed analytical model for CNN accelerators to enable an exploration of the design space of dense and sparse architectures. TimeLoop can model a wide range of data flows, including PT-IS-CP-dense, PT-IS-CP-sparse and others. Architecture parameters to TimeLoop include the memory hierarchy configuration (buffer size and location), ALU count and partitioning, and dense/sparse hardware support. TimeLoop analyzes the input data parameters, the architecture, and the dataflows, and computes the number of cycles to process the layer based on a bottleneck analysis and the counts of ALU operations and accesses to different buffers in the memory hierarchy. We apply an energy model to the time loop events derived from the synthesis modeling to compute the overall energy required to execute the layer. TimeLoop also computes the overall area of the accelerator based on the inputs from the synthesis modeling. For SCNN, the area model includes all of the elements from the synthesizable SystemC implementation. For dense architectures, area is computed using area of the major structures (RAMs, ALUs, and interconnect) derived from the SystemC modeling.

Architecture configurations. Table IV summarizes the major accelerator configurations that we explore, including both dense and sparse accelerators. All of the accelerators employ the same number of multiply ALUs so that we can compare the performance of the accelerators with the same computational resources. The dense DCNN accelerator operates solely on dense weights and activations and employs a dataflow called PT-IS-DP-dense, which is a variant of the PT-IS-CP-dense data flow described in Section III that uses a *dot-product* as its inner core operation. The optimized DCNN-opt architecture has the same configuration as DCNN but employs two optimizations: (1) compression/decompression of activations as they are transferred out of/into DRAM, and (2) multiply ALU gating to save energy when a multiplier input is zero. The DCNN architecture is configured with 2MB of SRAM for holding inter-layer activations, and can hold all of them for AlexNet and GoogLeNet. The SCNN configuration matches the architecture described in Section IV, and includes a total of 1MB of IARAM + OARAM. Because the activations are compressed, this capacity enables all of the activation data for the two networks to be held on chip, without requiring DRAM transfers for activations. The larger VGGNet requires the activation data to be transferred in and out of DRAM. The area required for each accelerator is listed in the last column. While SCNN has smaller activation RAM capacity, its larger size is due to the accumulator buffers, as described in Section IV.

TABLE IV
CNN ACCELERATOR CONFIGURATIONS.

	# PEs	# MULs	SRAM	Area (mm^2)
DCNN	64	1024	2MB	5.9
DCNN-opt	64	1024	2MB	5.9
SCNN	64	1024	1MB	7.9

Benchmarks. To explore the sensitivity of the architectures to sparsity parameters, we employ a synthetic network where we can adjust the degree of sparsity of both weights and activations. As described in Section II, we use AlexNet and GoogLeNet for the bulk of our experiments. With respect to GoogLeNet, we primarily focus on the convolutional layers that are within the *inception* modules [28]. VGGNet is known to be over-parameterized, which results in an extremely large amount of inter-layer activation data (6 MB or about 4×) the largest GoogLeNet layer. However, we use VGGNet as a proxy for large input data (such has high-resolution images) to explore the implications of tiling data on the SCNN architecture in Section VI-D.

VI. EVALUATION

This section first evaluates the sensitivity of SCNN to the sparseness of weights and activations using a synthetic CNN benchmark. We then discuss the performance and energy-efficiency of SCNN versus a dense CNN accelerator, using real world CNN applications. For brevity, all the inception modules in GoogLeNet are denoted as IC_id in all of the figures discussed in this section.

A. Sensitivity to CNN Sparsity

To explore the efficacy of sparse versus dense architecture, we first measure performance and energy as a function of density of weights and activations. Using the TimeLoop analysis tool, we examine GoogLeNet as we artificially sweep the weight and activation densities together from 100% (fully dense) down to 10%. Figure 7 shows results on SCNN, DCNN, and DCNN-opt. On the x-axis, the total density is the product of the weight and activation density. For example, 0.5/0.5 represents the point where both weights and activations are 50% dense so the overall density is 25%. Figure 7a shows that at 100% density, SCNN achieves about 79% of the performance of DCNN because it suffers from multiplier underutilization (discussed shortly). SCNN starts to perform better than DCNN as density decreases to 85%, reaching a 24× improvement at 10% weight/activation density. This chart does not include DCNN-opt as the energy optimizations over DCNN do not affect performance.

Figure 7b first shows that DCNN-opt's energy optimizations of zero gating and DRAM traffic compression cause it to be better than DCNN at every level of density. These energy optimizations are surprisingly effective given that they have such a small effect on the design of the accelerator. At high density, SCNN is notably less energy efficient than

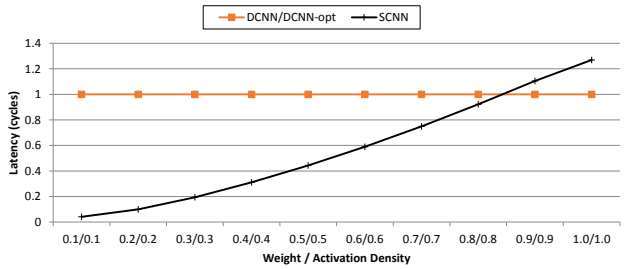

(a) Performance

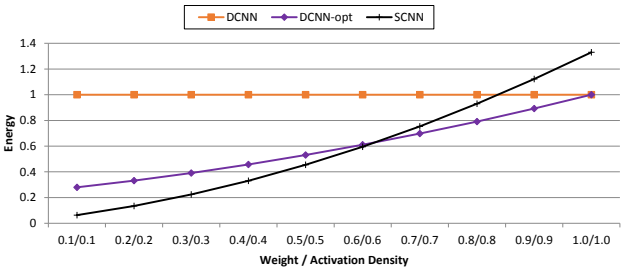

(b) Energy

Fig. 7. GoogLeNet performance and energy as a function of density.

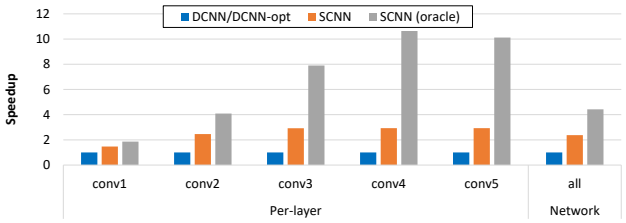

(a) AlexNet

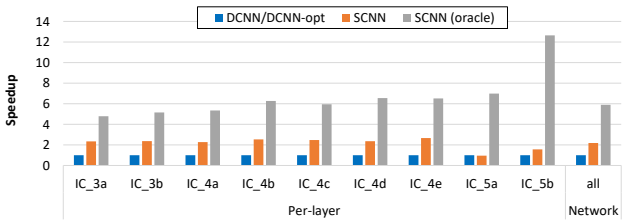

(b) GoogLeNet

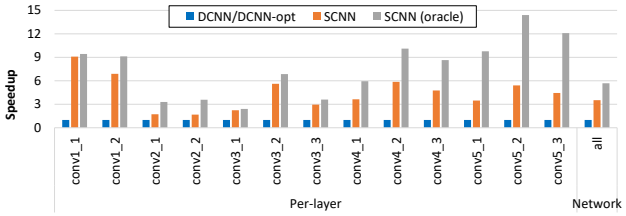

(c) VGGNet

Fig. 8. Performance.

either DCNN architecture due to the overheads of storing and maintaining the sparse data structures. SCNN becomes more efficient than DCNN at about 83% weight/activation density and more efficient than DCNN-opt at 60% density. Given the density measurements of the networks in Figure 1, we expect SCNN to outperform the dense architectures on nearly all of the layers of the networks we examined and be largely comparable in energy efficiency vs. DCNN-opt across these layers.

B. SCNN Performance and Energy

Performance. This subsection discusses the performance improvements offered by SCNN over the baseline dense DCNN accelerator. To demonstrate the upper-bound opportunity on performance, we also present the speedups offered by an *oracular* SCNN design (`SCNN(oracle)`). The performance of `SCNN(oracle)` is derived by dividing the number of multiplication operations required for Cartesian product-based convolution (Section III) with the number of multipliers available on-chip. Figure 8 summarizes the speedups offered by SCNN versus a dense CNN accelerator. Overall, SCNN consistently outperforms the DCNN design across all the layers of AlexNet, GoogLeNet, and VGGNet, achieving an average 2.37×, 2.19×, and 3.52× network-wide performance improvement, respectively.

The performance gap between SCNN versus `SCNN(oracle)` widens in later layers of the network, from left to right in the *x*-axis of Figure 8. The key reason behind this gap is closely related to each layer's average PE multiplier array utilization. In general, the working set allocated to each of the PEs in the later layers (e.g., `IC_5b`) are smaller than those in the earlier layers (e.g., `IC_3a`). As a result, it is more difficult to assign to a PE a sufficient number of non-zero activations and weights in the later layers to fully utilize the multiplier arrays.

Figure 9 quantitatively demonstrates this intra-PE fragmentation of the multiplier array. For the last two inception modules of GoogLeNet, the fragmentation issue becomes noticeably severe, with less than an average 20% multiplier utilization. In this layer 3 out of the 6 convolutional layers within the inception module have a filter size of 1×1, only having up to 8 non-zero weights within an output-channel group with a K_c value of 8. Nonetheless, the last layers generally account for a small portion of the overall execution time and SCNN generally provides significant performance improvement across the network. The right y-axis of Figure 9 demonstrates the effect of load imbalance across the PEs by showing the fraction of cycles spent waiting at inter-PE barrier. Overall, although the inter-PE global barriers and intra-PE fragmentation prevents SCNN from reaching similar speedups offered by oracular `SCNN(oracle)`, it still provides an average 2.7× performance over DCNN across the three state-of-the-art CNNs.

Energy-efficiency. Figure 10 compares the energy of the three accelerator architectures across the layers of the three networks. DCNN-opt improves energy efficiency by 2.0× over DCNN, while SCNN increases average efficiency by 2.3×. The behavior across the layers varies widely depending on the density of the layer, ranging from 0.89× to 4.7× improvement over DCNN and 0.76× to 1.9× improvement over DCNN-opt. Input layers such as VGGNet_conv1_1 and AlexNet_conv1

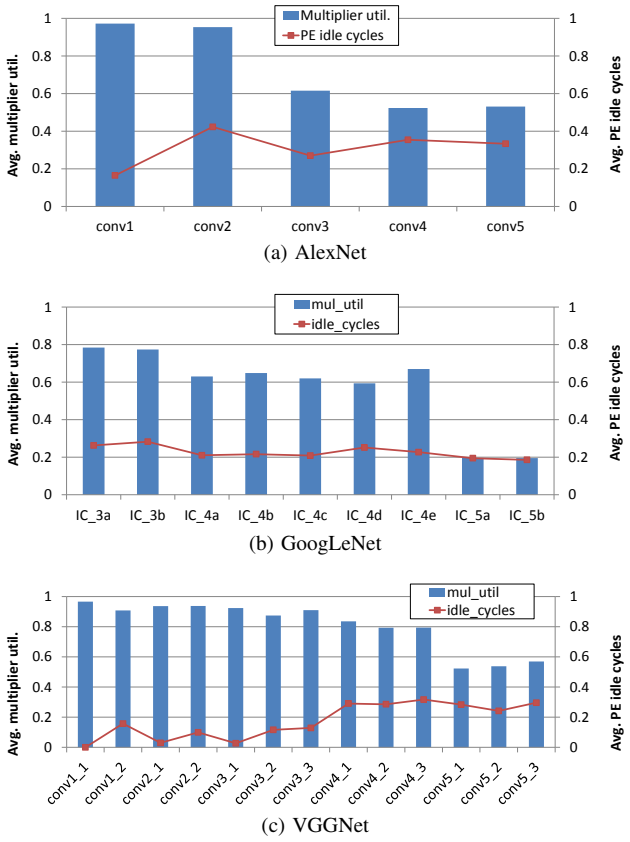

Fig. 9. Average multiplier array utilization (left-axis) and the average fraction of time PEs are stalled on a global barrier (right-axis), set at the boundaries of output channel groups.

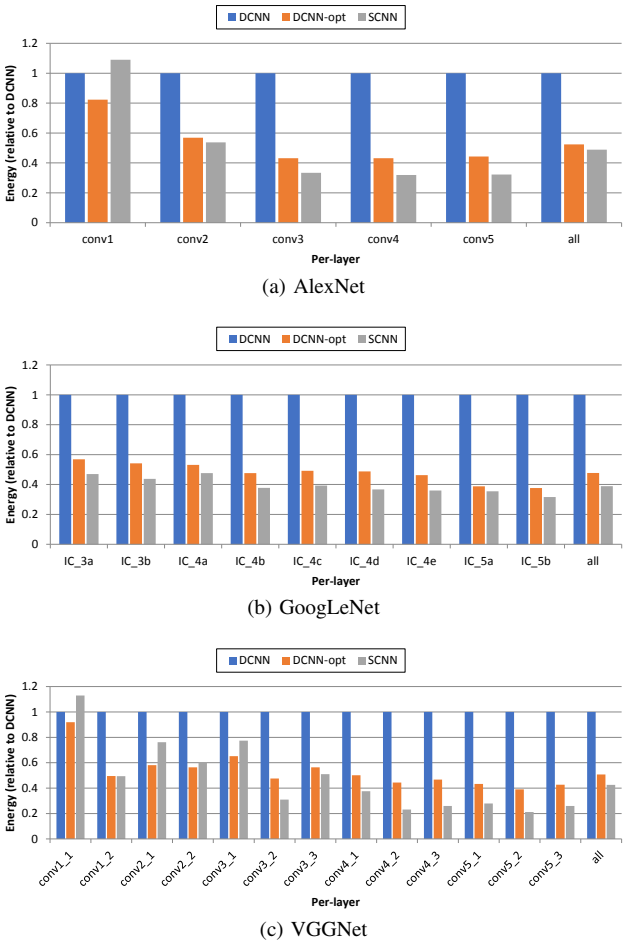

Fig. 10. Energy-efficiency.

usually present a challenge for sparse architectures because of their 100% input activation density. In such cases, the overheads of SCNN's structures such as the crossbar and distributed accumulation RAMs overshadow any benefits from fewer arithmetic operations and data movement.

C. PE Granularity

As outlined in Section VI-B, both cross-PE global barriers and intra-PE multiplier array fragmentation can contribute to degradation in the performance of SCNN. We quantify the effects of both of these factors on system performance by conducting the following sensitivity study. Assuming a fixed, chip-wide math throughput of 1,024 FLOPS, we sweep the total number of PEs on-chip from 64 (8×8 PEs, 16 multipliers per PE) down to 4 (2×2 PEs, 256 multipliers per PE). Clearly, an SCNN with 4 PEs can better sustain the effects of the global barriers than an SCNN with 64 PEs. However, the 4 PE configuration is also more likely to suffer from intra-PE fragmentation because each PE must now process a larger working set to fully utilize the math units. When evaluated on GoogLeNet, SCNN with 64 PEs achieves an 11% speedup than the one with 4 PEs as it does a better job utilizing the math arrays (average 59% math utilization versus 35%). We observed similar trends for AlexNet and VGGNet, concluding that addressing intra-PE fragmentation is more critical than inter-PE barriers for system-wide performance under our PT-IS-CP-sparse dataflow.

D. Larger Networks

SCNN is at its most efficient when it can capture all of the activations in its IARAM and OARAM. For a network with large layers like VGGNet, there are two choices. First, the designer could choose to provision SCNN with IARAM and OARAM large enough to hold the largest layer. While this approach would make processing the large layers more efficient by avoiding off-chip DRAM accesses, smaller layers would be penalized by incurring larger on-chip access overheads to RAMs that are larger than necessary. The second choice is to employ a tiling approach as described in Section IV. Our results show that this is only required for 9 of the 72 total evaluated layers, and for these 9 layers the overall energy penalty for shuttling the activation data to and from DRAM ranges from 5–62%, with a mean of 18%. While the tiling approach is attractive, we expect that there will be low power deployment scenarios that will motivate the designers of the neural networks to size them so that they fit in the on-chip SRAM capacity provided by the accelerator implementation.

VII. Related Work

Previous efforts to exploit sparsity in CNN accelerators have focused on reducing energy or saving time, which will invariably also save energy. Eliminating the multiplication when an input operand is zero is a natural way to save energy. Eyeriss [7] gates the multiplier when it sees an input activation of zero. For non-pruned networks the sparsity of weights is a less significant factor, and Eyeriss opted not to gate the multiplier on zero weights. This approach will save energy, but not save cycles. SCNN also saves energy by eliminating all the unnecessary multiplications, but doesn't even prepare to do a multiplication when any input operand is zero, thus saving time as well.

Another approach to reducing energy is to reduce data transfer costs when the data is sparse. Eyeriss uses a run length encoding scheme when transferring activations to and from DRAM. This saves energy (and time) by reducing the number of DRAM accesses. However, after the data is loaded into the on-chip buffer the data is stored in expanded form. Thus, there is no savings on data transfers from one internal buffer to another internal buffer or to the multipliers. SCNN also uses a compressed representation for all data coming from DRAM, but also maintains that compressed representation in the on-die buffers.

Another CNN accelerator designed to exploit sparsity, Cnvlutin [1] compresses activation values. However, it does not compress weights. Cambricon-X [30], does not compress the data coming from DRAM. Nor does it keep activations in a compressed form in the internal buffers, except in the queues directly delivering activations to the multipliers. Cambricon-X does keep only non-zero weights in the internal buffers. In contrast, SCNN keeps both weights and activations in a compressed form in both DRAM and internal buffers. This saves data transfer time and energy on all data transfers and allows the chip hold larger models for a given amount of internal storage.

Not delivering zero activation values or zero weights to the multipliers can save time by avoiding cycles when the multiplier has nothing to do. Cnvlutin selects only non-zero activation values for delivery as multiplier operands, but does occupy a multiplier with zero weights. Cambricon-X does not deliver either zero activations or weights to the multipliers. SCNN also does not deliver either zero activations or weights to the multipliers.

Finally, the EIE CNN accelerator [13] uses a compressed representation of both activations and weights, and only delivers non-zero operands to the multipliers. However, EIE is designed for the fully connected layers of a CNN model, while SCNN is targeting the convolutional layers where the majority of the computations are [9].

VIII. Conclusion

This paper presents the Sparse CNN (SCNN) accelerator architecture for inference in convolutional neural networks. SCNN exploits sparsity in both weights and activations using the *PlanarTiled-InputStationary-CartesianProduct-sparse* (PT-IS-CP-sparse) dataflow. This approach enables SCNN to use a novel Cartesian product-based computation architecture that maximizes reuse of weights and activations within a set of distributed processing elements. In addition, it allows the use of a dense compressed representation for both weights and activations to be used through almost the entire processing flow. This approach reduces data movement and on-die storage capacity relative to alternative architectures. Our results show that the SCNN architecture starts to beat a dense architecture in performance and energy efficiency when the weights and activations are each less than 85% dense. On three contemporary networks (AlexNet, GoogLeNet, and VGGNet) SCCN achieves performance improvements over the dense architecture by a factor of 2.7× while still being energy-efficient by a factor of 2.3×.

References

[1] J. Albericio, P. Judd, T. Hetherington, T. Aamodt, N. E. Jerger, and A. Moshovos. Cnvlutin: Ineffectual-Neuron-Free Deep Convolutional Neural Network Computing. In *Proceedings of the International Symposium on Computer Architecture (ISCA)*, pages 1–13, June 2016.

[2] D. Amodei, R. Anubhai, E. Battenberg, C. Case, J. Casper, B. Catanzaro, J. Chen, M. Chrzanowski, A. Coates, G. Diamos, E. Elsen, J. Engel, L. Fan, C. Fougner, T. Han, A. Hannun, B. Jun, P. LeGresley, L. Lin, S. Narang, A. Ng, S. Ozair, R. Prenger, J. Raiman, S. Satheesh, D. Seetapun, S. Sengupta, Y. Wang, Z. Wang, C. Wang, B. Xiao, D. Yogatama, J. Zhan, and Z. Zhu. Deep Speech 2: End-To-End Speech Recognition in English and Mandarin. https://arxiv.org/abs/1512.02595, 2015.

[3] Caffe. http://caffe.berkeleyvision.org, 2016.

[4] Caffe Model Zoo. https://github.com/BVLC/caffe/wiki/Model-Zoo, 2017.

[5] T. Chen, Z. Du, N. Sun, J. Wang, C. Wu, Y. Chen, and O. Temam. DianNao: A Small-footprint High-throughput Accelerator for Ubiquitous Machine-learning. In *Proceedings of the International Conference on Architectural Support for Programming Languages and Operation Systems (ASPLOS)*, pages 269–284, March 2014.

[6] Y.-H. Chen, J. Emer, and V. Sze. Eyeriss: A Spatial Architecture for Energy-Efficient Dataflow for Convolutional Neural Networks. In *Proceedings of the International Symposium on Computer Architecture (ISCA)*, pages 367–379, June 2016.

[7] Y.-H. Chen, T. Krishna, J. Emer, and V. Sze. Eyeriss: An Energy-efficient Reconfigurable Accelerator for Deep Convolutional Neural Networks. In *Proceedings of the International Solid State Circuits Conference (ISSCC)*, February 2016.

[8] R. Collobert, J. Weston, L. Bottou, M. Karlen, K. Kavukcuoglu, and P. Kuksa. Natural Language Processing (Almost) From Scratch. https://arxiv.org/abs/1103.0398, 2011.

[9] J. Cong and B. Xiao. Minimizing Computation in Convolutional Neural Networks. In *Proceedings of the International Conference on Artificial Neural Networks (ICANN)*, pages 281–290, September 2014.

[10] G. Diamos, S. Sengupta, B. Catanzaro, M. Chrzanowski, A. Coates, E. Elsen, J. Engel, A. Hannun, and S. Satheesh. Persistent RNNs: Stashing Recurrent Weights On-Chip. In *Proceedings of the International Conference on Machine Learning (ICML)*, June 2016.

[11] Z. Du, R. Fasthuber, T. Chen, P. Ienne, L. Li, T. Luo, X. Feng, Y. Chen, and O. Temam. ShiDianNao: Shifting Vision Processing Closer to the Sensor. In *Proceedings of the International Symposium on Computer Architecture (ISCA)*, pages 92–104, June 2015.

[12] A. Graves and J. Schmidhuber. Framewise Phoneme Classification With Bidirectional LSTM and Other Neural Network Architectures. In *Neural Networks*, 2005.

[13] S. Han, X. Liu, H. Mao, J. Pu, A. Pedram, M. Horowitz, and B. Dally. EIE: Efficient Inference Engine on Compressed Deep Neural Network. In *Proceedings of the International Symposium on Computer Architecture (ISCA)*, pages 243–254, June 2016.

[14] S. Han, H. Mao, and W. J. Dally. Deep Compression: Compressing Deep Neural Networks with Pruning, Trained Quantization and Huffman Coding. https://arxiv.org/abs/1510.00149, 2015.

[15] S. Han, J. Pool, J. Tran, and W. J. Dally. Learning Both Weights and Connections for Efficient Neural Networks. In *Proceedings of the International Conference on Neural Information Processing Systems (NIPS)*, pages 1135–1143, December 2015.

[16] A. Hannun, C. Case, J. Casper, B. Catanzaro, G. Diamos, E. Elsen, R. Prenger, S. Satheesh, S. Sengupta, A. Coates, and A. Y. Ng. Deep Speech: Scaling Up End-To-End Speech Recognition. https://arxiv.org/abs/1412.5567, 2014.

[17] K. He, X. Zhang, S. Ren, and J. Sun. Deep Residual Learning for Image Recognition. https://arxiv.org/abs/1512.03385, 2015.

[18] G. Huang, Y. Sun, Z. Liu, D. Sedra, and K. Weinberger. Deep Networks with Stochastic Depth. https://arxiv.org/abs/1603.09382, 2016.

[19] ImageNet. http://image-net.org, 2016.

[20] A. Krizhevsky, I. Sutskever, and G. E. Hinton. ImageNet Classification with Deep Convolutional Neural Networks. In *Proceedings of the International Conference on Neural Information Processing Systems (NIPS)*, December 2012.

[21] Y. LeCun, Y. Bengio, and G. Hinton. Deep Learning. *Nature*, 521:436–444, May 2015.

[22] G. Martin and G. Smith. High-Level Synthesis: Past, Present, and Future. *IEEE Design & Test of Computers*, 26(4):18–25, July/August 2009.

[23] Catapult High-Level Synthesis. https://www.mentor.com/hls-lp/catapult-high-level-synthesis, 2017.

[24] NVIDIA cuDNN. https://developer.nvidia.com/cudnn, 2016.

[25] B. Reagen, P. Whatmough, R. Adolf, S. Rama, H. Lee, S. Lee, J. M. H. Lobato, G.-Y. Wei, and D. Brooks. Minerva: Enabling Low-Power, High-Accuracy Deep Neural Network Accelerators. In *Proceedings of the International Symposium on Computer Architecture (ISCA)*, pages 267–278, June 2016.

[26] M. Rhu, N. Gimelshein, J. Clemons, A. Zulfiqar, and S. W. Keckler. vDNN: Virtualized Deep Neural Networks for Scalable, Memory-Efficient Neural Network Design. In *Proceedings of the International Symposium on Microarchitecture (MICRO)*, October 2016.

[27] K. Simonyan and A. Zisserman. Very Deep Convolutional Networks for Large-Scale Image Recognition. https://arxiv.org/abs/1409.1556, May 2015.

[28] C. Szegedy, W. Liu, Y. Jia, P. Sermanet, S. Reed, D. Anguelov, D. Erhan, V. Vanhoucke, and A. Rabinovich. Going Deeper with Convolutions. In *Proceedings of the Conference on Computer Vision and Pattern Recognition (CVPR)*, June 2015.

[29] Wired. Microsoft Neural Net Shows Deep Learning Can Get Way Deeper, 2016.

[30] S. Zhang, Z. Du, L. Zhang, H. Lan, S. Liu, L. Li, Q. Guo, T. Chen, and Y. Chen. Cambricon-X: An Accelerator for Sparse Neural Networks. In *Proceedings of the International Symposium on Microarchitecture (MICRO)*, October 2016.